The Dynamics of H + $HeH^+(v = 0, j = 0) \rightarrow H_2^+$ + He: Insight on the Possible Complex-forming Behaviour of the Reaction

Tomás González-Lezana*

Instituto de Física Fundamental, C.S.I.C., Serrano 123, Madrid 28006, Spain

Duncan Bossion and Yohann Scribano

Laboratoire Univers et Particules de Montpellier, Université de Montpellier, LUPM - UMR CNRS 5299, 34095 Montpellier Cedex, France

Somnath Bhowmick and Yury V. Suleimanov

Computation-based Science and Technology Research Center, The Cyprus Institute, 20 Konstantinou Kavafi Street, Nicosia 2121, Cyprus

Abstract

The H + $HeH^+ \rightarrow$ He + H_2^+ reaction has been studied by means of a combination of theoretical approaches: a statistical quantum method (SQM), ring polymer molecular dynamics (RPMD) and the quasiclassical trajectory (QCT) method. Cross sections and rate constants have been calculated in an attempt to investigate the dynamics of the process. The comparison with previous calculations and experimental results reveals that despite statistical predictions seem to reproduce some of the overall observed features, the analysis at a more detailed state-to-state level shows noticeable deviations from a complex-forming dynamics. We find some differences in cross sections and rate constants obtained in the QCT calculation with a Gaussian binning procedure with respect to previous works in which the standard histogram binning was employed.

*t.gonzalez.lezana@csic.es

I. INTRODUCTION

The importance of the helium hydride ion HeH^+ in the early Universe chemistry, being one of the first bond to form by radiative association with protons and playing a crucial role in the formation of molecular hydrogen [1], explains the interest on the study of those reactive processes in which this species takes part. Thus for instance, H + HeH^+ → He +H_2^+ [2–6] and the corresponding reverse reaction, [7–9] have been the subject of a number of both theoretical and experimental investigations over the years.

Quasiclassical trajectory (QCT) calculations have focussed on the stereodynamics of the H + HeH^+ reaction and the possible isotopic effect when one of the hydrogen atom is substitued either by D or T [10]. Cross sections, on the other hand, have been calculated by means of QCT and quantum mechanical (QM) approaches covering an ample range of collision energies [4–6, 11].

Due to its relevance in the primordial chemistry affecting the cosmic microwave background [12] and the consumption of HeH^+ [13] the rate constant of the title reaction has been subject of study before. In their study of the chemistry of the early universe, Galli and Palla [14] simply adopted a constant temperature independent value of 9.1 $\times 10^{-10}$ cm^3 s^{-1}, equal to about one-half of the Langevin collision rate constant, in order to agree with the earlier ion cyclotron resonance measurement performed by Karpas *et al.* [15] at $T = 300$ K. Schleicher *et al.* [12] proposed an analytical fit for a temperature range between 100 K and 10^5 K to the rate constant obtained by numerical integration of cross sections reported in Ref. [16]. More recent investigations have reported values of the rate constant for the H + HeH^+ → He + H_2^+ reaction for a wide range of temperatures [2–4].

Various potential energy surfaces (PESs) have been developed since the late 70s in order to describe the interaction which governs the corresponding reactive scattering processes [17–23]. One of the most noticeable features of the system is the existence of a potential energy minimum about 1.09 eV below the HeH^+ + H arrangement and 0.35 eV below the He + H_2^+ channel which corresponds to a stable intermediate HeH_2 collinear species [23]. The value of this potential well depth is therefore of the same order of magnitude of some other related reactive systems involving a diatomic ion formed with hydrogen and a rare gas atom such as $HeHeH^+$ ($\sim$ 0.7 eV) or $HeNeH^+$ ($\sim$ 0.5 eV). In previous investigations the dynamics of these processes have been studied by a combination of theoretical methods

which included statistical techniques [24–27]. These approaches assume the formation of an intermediate complex between reactants and products and therefore one can learn a lot about the actual dynamics of the process analyzing the performance of these methods. In the above mentioned reactions, Ne+NeH^+, Ne + HeH^+ and He + NeH^+, the agreement of predictions from a statistical quantum method (SQM) with both QM and QCT results were found to depend in some cases on the collision energy range under consideration, the value of the total angular momentum or the initial rovibrational state of the corresponding reactant diatom. In this work we have employed such a SQM method [28–30] in combination with QCT and ring polymer molecular dynamics (RPMD) using the PES of Ramachandran *et al.* [23] to study the dynamics of the H + $HeH^+ \rightarrow$ He + H_2^+.

The structure of the paper is as follows: First we show the details of the theoretical methods employed in the calculations; then we will present and discuss the results and we end with the corresponding conclusions.

II. METHODS

A. Statistical Quantum Method

The present statistical method [28–30] has been successfully applied to study atom-diatom complex-forming reactions involving collisions with, for example, H_2 [31] or O_2 [32, 33]. Investigations on reactions involving rare gas atoms such as Ne or He and H [24, 27] were carried out by means of statistical predictions in comparison with exact QM results.

The state-to-state reaction probability $P^J_{v,j;v'j'}(E_c)$ for a specific value of the total angular momentum J can be approximated within the context of the statistical approach as follows:

$$P^J_{v,j;v'j'}(E_c) = \mid S^J_{v,j;v'j'}(E_c) \mid^2 \simeq \frac{p^J_{v,j}(E_c) p^J_{v'j'}(E_c)}{\sum_{v''j''} p^J_{v''j''}(E_c)}, \tag{1}$$

where $p^J_{v,j}(E_c)$ and $p^J_{v'j'}(E_c)$ correspond to capture probabilities for the formation of the complex from the $HeH^+(v,j)$ initial state and its subsequent fragmentation to the $H_2^+(v',j')$ final state at the collision energy E_c. The sum on the denominator of Eq. 1 runs for all energetically open states from both reactants and products arrangements. The corresponding integral cross section (ICS) is obtained by means of the standard partial wave average [29] of the above mentioned state-to-state reaction probability $P^J_{v,j;v'j'}(E_c)$ and the rate constant

is computed by integration of the cross section on a Boltzmann distribution. The maximum value of the total angular momentum $J_{\max}$ required for these calculations is 45.

The statistical calculation were performed both under the centrifugal sudden (CS) approximation and within a coupled-chanel scheme to solve the corresponding log derivative propagation. Comparisons between both approaches revealed noticeable differences which suggested the convenience of discarding the numerical cheaper CS version.

The values of the capture $R_{\min}$ and asymptotic $R_{\max}$ radii defining the region in which the calculation is performed are, for the H+HeH^+ arrangement, 1.57 Å and 36.67 Å; and for the product He+H_2^+, 1.28 Å and 29.0 Å, respectively.

B. Quasiclassical Trajectory Method

The QCT calculations were performed solving classical Hamiltonian equations the details on the methodology can be found in our previous papers [34, 35] as well as other well known papers [37, 38]. In this work, we have taken into account the zero-point energy (ZPE) leakage, using a scheme based on the Gaussian binning (GB) procedure proposed by Bonnet and Rayez [39]. In their original work, Bonnet and Rayez have proposed this weighted trajectories scheme for transition between pure vibrational levels. Later, Bonnet and Espinosa-Garcia [40] have shown that for transitions between rovibrational levels, the results obtained with the GB procedure for both pseudo quantum numbers $(\tilde{\nu}, \tilde{j})$ are very similar to the ones obtained with a GB scheme for the pseudo-vibrational quantum number $\tilde{\nu}$ and a histogram binning (HB) scheme for the pseudo-rotational quantum number $\tilde{j}$. This good agreement can be simply explained by the high density of rotational levels for a given vibrational level such that the energy spacing between different rotational levels is too small for the GB to change the global assignment of rotational quantum numbers. We thus follow this simplified strategy by GB-weighting the vibrational pseudo-quantum number and we use a standard HB weighting scheme for pseudo-rotational quantum number.

As in the GB procedure, each trajectory associated to the vibrational pseudo quantum number $\tilde{\nu}$ is weighted by the factor $e^{-\frac{(\tilde{\nu}-\nu')^2}{2\varsigma^2}}$ where ς is the variance. We have propagated a large number of trajectories for a given initial rovibrational state (ν, j) and at a fixed collisional energy E_c. At the end of the propagation, trajectories leading to a product arrangement γ were analyzed with an attribution of their pseudo vibrational $\tilde{\nu}$ and rotational $\tilde{j}$

quantum numbers using the semiclassical Wentzel-Kramers-Brillouin quantization condition [36].

We thus determine the number of trajectories $\mathcal{N}_r^{(\gamma)}(\nu',\ j';E_c)$ for a given channel γ leading to the final rovibrational quantum number (ν', j') state as :

$$\mathcal{N}_r^{(\gamma)}(\nu',\ j';E_c) = \sum_{i=1} e^{-\frac{(\tilde{\nu}_i-\nu')^2}{2\varsigma^2}} \Pi(\tilde{\nu}_i-\nu')\Pi(\tilde{j}_i-j^{'}) \tag{2}$$

where i is a label running over trajectories leading to this γ channel and where we consider the property of rectangular function $\Pi(\tilde{\xi}-\xi^{'}) = 1$ if $|\tilde{\xi}-\xi^{'}| \leq 1/2$ and 0 otherwise. In the above equation, the variance ς was chosen in order to get a 0.1 value of the full width at half maximum. We obtain the reaction probability to a given channel γ and for the final rovibrational state (ν', j') as usual :

$$P^{(\gamma)}(\nu, j \rightarrow \nu',\ j';E_c) = \frac{\mathcal{N}_r^{(\gamma)}(\nu',\ j';E_c)}{\mathcal{N}_{tot}(\nu,j;E_c)} \quad \text{with} \quad \mathcal{N}_{tot}(\nu,j;E_c) = \sum_{\nu',\ j',\gamma} \mathcal{N}_r^{(\gamma)}(\nu',\ j';E_c) \tag{3}$$

and where the dissociation channel was not considered in the calculation of the total number of trajectories $\mathcal{N}_{tot}(\nu,j;E_c)$ as the total energy considered in this study is below dissociation limit. We have also properly normalised the number of our trajectories using a specific-channel normalisation factor. This normalization step was done in a way to conserve the number of trajectories which do not violate the ZPE for a given channel. This distinction of trajectories, violating/or not ZPE, in the calculation of the normalization factor, presents the advantage to reduce the impact of a possible too low statistic of the trajectory sampling. With Eq.3, we determine the state-to-state cross section for a given channel γ :

$$\sigma^{(\gamma)}_{\nu',j'\leftarrow\nu,j}(E_c) = \pi b_{\max}^2 P^{(\gamma)}(\nu, j \rightarrow \nu', j';E_c) \tag{4}$$

where $b_{\max}$ is the maximal impact parameter determined by running small batches of trajectories. This maximal impact parameter was considered reached when there was no more reaction, and inelastic trajectories had $|\tilde{j}-j| \leq 0.45$.

We also obtained the median $\tau_{1/2}$ and average lifetime $\bar{\tau}$ of the intermediate complex at a state-to-state level or for a specific initial or final state. Each trajectory has his own intermediate complex lifetime τ_i (we consider the highest possible value τ_i^{max} for a given trajectory which can meet several times this criteria) which is evaluated when the three internuclear distances are bellow a fixed distance criterion (here this distance is taken to

5 bohrs which corresponds to the maximal internuclear distance when the complex in linear configuration is formed). At the end of the propagation, the median and average of all the lifetimes over the total considered trajectories for a given process (state-to-state or state specific level for a given channel) is evaluated.

We propagate 100 000 trajectories per collisional energy from 0.8 meV to 0.9 eV by energy-steps of 8 meV, the initial atom-diatom distance being 30 bohrs.

C. Ring Polymer Molecular Dynamics

The RPMD method takes advantages of the isomorphism between the quantum statistical mechanics of a quantum system and the classical statistical mechanics of a fictitious ring polymer. This ring polymer is composed of copies of the original system (beads) connected by harmonic springs. Hence, RPMD is classical molecular dynamics in an extended n-beads imaginary time path integral phase space [41]. It has been proven to be a very reliable method to study bimolecular reaction of insertion type such as typical atom-diatoms with a well [42] and a very complete description of the method can be found in Refs. [43, 44]. The Hamiltonian in cartesian coordinates of a system of N atoms with fictitious ring polymers of n beads in atomic units is :

$$H_n(\mathbf{p},\mathbf{q}) = \sum_{i=1}^{N}\sum_{j=1}^{n}\left(\frac{{p_i^{(j)}}^2}{2m_i} + \frac{1}{2}m_i\omega_n^2\left|q_i^{(j)} - q_i^{(j-1)}\right|^2\right) + \sum_{j=1}^{n} V(q_1^{(j)}, q_2^{(j)}, ..., q_N^{(j)}) \tag{5}$$

with $q_i^{(j)}$ and $p_i^{(j)}$ the position and momenta of the j-th bead of the i-th atom of the system, and $q_i^{(0)} \equiv q_i^{(n)}$. The force constant of the harmonic springs is $\omega_n = \beta\hbar/n$ and $\beta = 1/k_BT$ with the temperature T of the system. We introduce a dividing surface $s(\mathbf{q}) = \mathbf{0}$ between reactants and products, products being in $s > 0$ and the reaction coordinate $\bar{s}(\mathbf{q}) = \mathbf{s}(\bar{\mathbf{q}}_\mathbf{1}, ..., \bar{\mathbf{q}}_\mathbf{N})$ with the centroid variables :

$$\bar{q}_i = \frac{1}{n}\sum_{j=1}^{n} q_i^{(j)} \tag{6}$$

As explained in Suleimanov et al. [45], the method uses a two dividing surfaces formalism that we briefly recall below. The ring polymer flux-side correlation function c_{fs} that leads to the rate constant calculation when $t \to \infty$ is a real and odd function of t with a discontinuity at $t \to 0_+$. It allows in this limit to define the transition state theory approximation, which

is an upper bound to the RPMD rate. We can express the RPMD rate constant as :

$$k^{RPMD}(T) = \kappa(s_1)k^{QTST}(s_1) = \kappa(s_1)p(s_1, s_0)k^{QTST}(s_0) \tag{7}$$

The dividing surface s_1 is situated in the transition state region, the second dividing surface is localized in the asymptotic reactant valley and is defined as $s_0(\bar{\mathbf{q}}) = R_\infty - |\bar{\mathbf{R}}| = 0$, $\bar{\mathbf{R}}$ being the centroid of the Jacobi vector that connects the center of mass of the two reactants. The first factor is a n-beads ring polymer transmission coefficient for a dividing surface in the region of the reaction barrier :

$$\kappa(s_1) = \frac{c_{fs}(t \to \infty; s_1)}{c_{fs}(t \to 0_+; s_1)} \tag{8}$$

Here, c_{fs} is the flux-side correlation function. The second factor is the ratio of ring polymer transmission coefficients with two different dividing surfaces :

$$p(s_1, s_0) = \frac{c_{fs}(t \to 0_+; s_1)}{c_{fs}(t \to 0_+; s_0)}. \tag{9}$$

It could also be expressed in terms of the centroid potential of mean force (PMF) [44], $W(s)$:

$$p(s_1, s_0) = e^{-\beta[W(s_1) - W(s_0)]}. \tag{10}$$

$W(s)$ is related to the probability distribution function $P^{(n)}(s)$ as:

$$W(s) = -\frac{1}{\beta} \ln P^{(n)}(s) \tag{11}$$

The third term is expressed as :

$$k^{QTST}(s_1) \;=\; 4\pi R_\infty^2 \left(\frac{1}{2\pi\beta\mu_R}\right)^{1/2} e^{-\beta[W(s_1) - W(s_0)]}, \tag{12}$$

$$k^{QTST}(s_0) \;=\; 4\pi R_\infty^2 \left(\frac{1}{2\pi\beta\mu_R}\right)^{1/2}, \tag{13}$$

R_∞ being an asymptotic distance between reactants, large enough that no interaction takes place over it, μ_R is the reduced mass of the reactants. The calculations are run using the RPMDrate code [46] developed by one of us (Y. Suleimanov). We computed the RPMD rate constants with different values of R_∞ and the number of beads to ensure convergence. The centroid potential of mean force profile has been computed using the umbrella integration

procedure [47, 48], that bias the dynamics simulation, by dividing the reaction path coordinates into 111 equally spaced windows in the range $[-0.05; 1.05]$. The input parameters of the RPMD simulation can be found in Tab. I. In order to calculate the ring polymer transmission coefficient (Eq. 8), the recrossing trajectory evolution (with its centroid constrained at s_1) has been carried out for 2 ns after initial thermalization period of 20 ps in the presence of an Andersen thermostat [49].

III. RESULTS

A. Cross sections

The dependence of the ICS with the collision energy is shown in Figure 1 where present SQM and QCT-GB results are compared with both the QM and QCT-HB cross sections reported in Ref. [2] for an energy range between 10^{-5} eV and 0.7 eV. As discussed by Esposito *et al.*, the QCT calculation, the only numerically possible beyond 1 eV in their work [2], fails however for energies below $E_c \sim 0.05$ eV remaining clearly below the QM cross sections. The SQM ICS, in turn, exhibits a reasonably good agreement with the QM values for the energy range within 0.03 eV and 0.2 eV. For $E_c < 0.03$ eV, the statistical predictions only reproduce qualitatively the trend seen for the QM ICS as the energy decreases, but values are noticeably smaller. When $E_c > 0.2$ eV, the SQM cross sections decrease faster than both QM and QCT counterparts when the energy increases.

An example of an actual numerical comparison is shown in Table II, when values of the ICSs obtained with the SQM approach are compared with those obtained in the QCT and QM calculation of Ref. [2] at $E_c = 0.001$, 0.01 and 0.1 eV. The difference between the statistical and quantum cross sections of about a factor of ~ 2 found at $E_c = 0.001$ eV becomes even larger when lower values of the collision energy are considered.

The comparison of these theoretical results with existing experimental work reveals interesting features. In particular, Figure 1 shows present in a inset SQM cross sections besides the QM values reported in Ref. [2] and the measurements reported in the early work by Rutherford and Vroom [50] which extend up to ~ 3 eV. The statistical cross sections, below the QM results, are much closer however to those obtained in the beam apparatus experiment performed in Ref. [50] and even suggest the slight change in their trend with the

collision energy as approaching to $E_c = 1$ eV. The QCT cross sections shown in the inset of Figure 1, on the other hand, correspond to a calculation performed in this work applying the GB procedure.

The analysis of the state-to-state He + $HeH^+(v = j = 0) \rightarrow$ He + $H_2^+(v')$ reveals the different behaviour of each process depending on the final vibrational excitation of the product diatom $H_2^+(v')$. Thus, we notice in Figure 2 how the statistical cross sections for the production of $H_2^+(v' = 0)$ on its ground vibrational state overestimate the QM result [2] for the intermediate energy range 10^{-3} eV $\leq E_c \leq 0.4$ eV. It matches perfectly, on the contrary, the QM ICSs beyond the entire cold regime here considered $E_c < 10^{-3}$ eV down to 10^{-5} eV. For $H_2^+(v' = 1)$, the agreement between the QM and SQM calculations is seen however in the above mentioned intermediate energy range. The formation of H_2^+ in larger vibrationally excited states is clearly not well reproduced by statistical means. This distinct trend is due to certain specificity exhibited by the QM cross sections, which are slightly larger for $H_2^+(v' = 1, 2)$ and smaller for both $v' = 0$ and 3. Numerical values of these final vibrational state selected ICSs can be also checked in Table II at collision energies of $E_c = 0.001$, 0.01 and 0.1 eV.

Numerical values of the final vibrational state selected cross sections shown in Table II suggest a relevant issue which regards the actual comparison between the SQM results and both QM and QCT distributions. A tendency to exhibit some inversion, which yields either $v' = 2$ or 3 as the most populated vibrational state, is observed for the three energies in consideration in that Table. The QCT calculation, with the only exception of those energies close to the threshold for the reaction beyond $E_c = 0.001$ eV, seems to reproduce such a behaviour as the energy increases. It is clear, on the contrary, that the statistical predictions, which always favour the vibrational ground $H_2^+(v' = 0)$ level as the most populated state whereas the population for the other states $v' > 0$ in a monotonous decrease with v', do not provide the correct description of the vibrational distributions.

B. Rotational distributions

We have also calculated SQM and QCT rovibrational distributions for the H + $HeH^+(v = 0, j = 0) \rightarrow$ He + $H_2^+(v', j')$ reaction for specific values of the collision energy. Figure 3 shows the population of the different rovibrational states of the product $H_2^+(v', j')$ at $E_c = 57$ meV.

For that energy, the QCT method yields ICSs in good agreement with the QM results from Ref. [2] (see Figure 1). The statistical predictions remain slightly bigger but in a reasonable good accord. The comparison at the fine state-to-state level between the QCT and SQM results shown in Figure 3, reveals that the distribution among the different rotational states exhibits a statistical profile specially for $H_2^+(v' = 1)$. The formation of H_2^+ in its ground vibrational state however seems not to be ruled merely by statistical considerations: values obtained by means of the SQM approach are clearly larger than those calculated with the QCT method. More significant disagreement between both approaches is observed when the rovibrational distributions for $v' = 2$ and 3 (see bottom panel of 3) are compared.

A similar situation is found for a larger collision energy, $E_c = 0.16$ eV. The corresponding rovibrational cross sections obtained with our SQM and QCT calculations are shown in Figure 4. As for the previous energy under consideration, whereas QCT distributions for the formation of $H_2^+(v' = 1)$ are well reproduced by the statistical counterpart, SQM predictions for $v' = 0$ remain larger than the QCT cross sections. The two other vibrationally excited states, $v' = 2$ and 3, shown in the bottom panel of Fig. 4, display a perhaps better comparison between the QCT and SQM. In view of Figure 1 one supposes that perhaps more disagreement would be seen for larger energies. The analysis of the rovibrational distributions supports, on the other hand, the especially good accord found in the vibrational-state selected $H + HeH^+ \rightarrow He + H_2^+(v' = 1)$ process leading to the formation of H_2^+ in its first vibrationally excited state.

C. Centroid potentials of mean force and ring polymer transmission coefficient

The profiles of centroid PMF $W(\xi)$ as functions of the reaction coordinate, ξ, defined in terms of s_0 and s_1 (see, *e.g.*, Ref. [44]), at $T = 20$-600 K are plotted in Fig. 5(A). Apparently, there are two distinct variations along ξ, one at $T = 10$-75 K and the other one at higher temperatures ($T \geq 100$ K). For $T = 10$-75 K, the PMF profile is essentially barrierless and is a characteristic of ion-radical complex-forming reaction [51]. The profiles are virtually flat before entering the deep-well zone. The deep-well is located immediately after the very small thermodynamic maxima observed on these PMFs with a steep negative free energy gradient around it. At higher T (≥ 100 K), there is a steady decrease in the free energy values leading to the well. It is interesting to note that with the temperature increase, there

is a gradual increase in the thermodynamic barrier height in the corresponding PMFs that can reach up to 0.11 eV at 600 K. With the rise of temperature, the reaction coordinate where the formation of well takes place progressively moves to a higher value of ξ. The maximum in the PMF profile hovers within ξ = 0.74-0.80 for all the temperatures. The umbrella sampling trajectories were not propagated further towards the products side from the well.

The variation in the time-dependent transmission coefficient $\kappa(t)$ is depicted in Fig. 5(B). From these plots, it is clear that the recrossing does take place at all the temperatures, and therefore, it plays a crucial role in determining the final RPMD rate constant. A very long propagation time (1.5 ps) is required to converge the $\kappa(t)$ since the title reaction proceeds through a complex-forming mechanism. Similar to the PMF profiles, we can separate the characteristics of $\kappa(t)$ into two categories: one at low temperatures ($T \leq 75$ K) and the other for $T \geq 100$ K. In the first case, the plateau value of κ becomes large and is attained faster with the rise in temperature. This is maybe due to the greater capability of the RPMD (child) trajectories to enter and re-enter the complex forming zone at higher temperatures. Note that the plateau values of κ at $T = 50$ and 75 K are very similar. At higher temperatures ($T \geq 100$ K), after initial oscillations, $\kappa(t)$ attains constant value rapidly at around 500 fs. In contrast to the low temperature case, the plateau value of κ decreases with the increase in temperature. This seemingly opposite behaviour of $\kappa(t)$ with temperature is related to the barrier heights in the PMF profiles that increase with temperature for $T \geq 100$ K and is negligible at low temperatures. This phenomenon is previously observed for the C + H_2 reaction [52] and O + H_2 [53] reactions.

D. Rate constants

Rate constants as a function of the temperature calculated here with the SQM, QCT and RPMD methods have been compared with results previously reported in the literature. In particular, in Figure 6, values of present rates for a temperature range between 0 and 600 K are shown in comparison with the rate constant a T = 200 K measured in the ion cyclotron resonance experiment of Ref. [15]. This measurement is nicely reproduced by the QM rate constant of Esposito *et al.* [2] and its error bars extend sufficiently to also validate both the statistical and QCT predictions. It is worth noticing that present SQM

rate constant constitutes a fairly good alternative to the QM value, despite it remains larger for the entire temperature domain under consideration. In addition to this, Figure 6 also reveals that the GB procedure certainly introduces some improvement with respect to the rate constants obtained in the QCT calculation of Ref. [2] where authors employed instead the HB alternative.

Although the RPMD rate constant values for the low temperature regime $T \leq 100$ K are in a good agreement with both the QM calculation of Ref. [2] and the present SQM predictions, they remain larger for the higher temperatures. In particular, at $T = 200$ K, the RPMD value is just inside the upper limit of the error bar of the measurement reported by Karpas *et al.* [15]. A possible explanation for this discrepancy, particularly at high temperatures, may lie in the fact that the interaction potential of the activated reactants at s_0 is not minimized by the chosen value of R_∞.

The comparison also includes the rate constants reported in Refs. [12] and [13], originally obtained for a much wider temperature range (100 K $< T < 10^5$ K) and commonly employed in Astrophysical models. Although actual values are not really that different than those calculated with the present methods, the trend of the rate constants as the temperature increases is not the same.

As discussed in the previous sections with ICSs as a function of the energy, we are interested here in analysing the behaviour of the rate constants at a much finer state-to-state detail. Thus, we have employed the SQM and QCT methods to obtain the thermal rates for the corresponding He + $HeH^+(v = 0, j = 0) \rightarrow H_2^+(v')$+He processes in which the final vibrational state of $H_2^+(v')$ is specified. In Figure 7 we compare present results for $H_2^+(v' = 0 - 3)$ with those obtained in the QM and QCT calculations reported by Esposito *et al.* [2]. It is now again clear that the only case in which all rate constants are in a remarkably good agreement is for the formation of H_2^+ in its first vibrationally excited state $v' = 1$. In the other cases, the statistical predictions remain clearly above ($v' = 0$) or below ($v' = 2, 3$) both the QM and QCT results. It then seems that the apparent good accord with the QM rate constants seen in Figure 6 is result of a sort of averaged balance among all vibrational states, even if the SQM approach is far to provide the right description of the process for some of them. Whereas the statistical prediction favours the production of the HeH^+ in its ground vibrational state and yields decreasing rate constants as final vibrational excitation increases, both QCT and QM point out certain inversion in favour

of the $v' = 1$ case. Present results also suggest the convenience of the GB procedure in the QCT calculations since the state-to-state rate constants shown in Figure 7 obtained in such way differ from those obtained with the HB alternative [2] given the slightly better agreement with the QM counterparts.

IV. DISCUSSION

The analysis of the collision complex lifetime obtained with the QCT approach also gives some further indication of the dynamics of the process. The dependence with the collision energy reveals that lifetimes display a maximum value which remains slightly fluctuating between 30 and 40 fs eV at 0.002 eV $\leq E_c \leq$ 0.08 eV. For higher collision energies the calculated lifetime starts to decrease. This sudden change suggests that the dynamics of the process is shifting to a direct pathway which does not necessarily involves the formation of an intermediate complex between reactants and products. Therefore this would explain the deviations observed for the statistical ICSs in comparison with the QM and QCT results (see Figure 1) which remain larger for the highest energies here considered. Estimation of such a lifetime for product vibrational state selected processes shown in Figure 7 does not lead however to significant differences depending on the specific $H_2^+(v')$. Thus the apparent better agreement of the SQM predictions with both QM and QCT ICSs for the formation of vibrationally excited $H_2^+(v' = 1, 2)$ as compared with the $v' = 0$ and 3 cases can not be explained in terms of longer lifetimes for the corresponding intermediate complex. In any case, the actual values of such lifetimes, 40-50 fs at maximum, certainly suggest that the departure from a purely statistical behaviour is clearly an expectable result.

ICSs reported in Ref. [4] included the Langevin expression calculated in terms of the dipole polarizability of the incoming atom, the vacuum electricity constant and the collision energy. The comparison with the corresponding QM result revealed a clear overestimation of this capture cross section over the entire collision energy there considered ($E_c \leq 800$ meV). This is clearly at odds with respect to our present findings which indicate that the SQM predictions are, in general, below the QM cross sections. But the most striking difference with the trend followed by the Langevin cross section shown by De Fazio [4] regards the behaviour at the low energy regime. Although a detailed inspection can not be seen from Fig. 2 of Ref. [4] it seems clear that the Langevin result is far to reproduce the QM cross

section at low energies, a feature which is clearly seen on the contrary for the SQM cross sections.

Present results exhibit a clear distinct behaviour with the temperature (at the $T \leq 600$ K range) as compared with those rate constants employed in an astrophysical context, that is, those from Refs. [13] and [12]. The trend shown by these two sets of data is clearly smoother as the temperature increases, whereas both present rate constants and those reported in Ref. [2] display a much more marked dependence with T, especially for the lowest values. At $T \sim 600$ K a suggested tendency to stabilize in a nearly constant value of the rate constant lead to the QM, QCT and stastistical predictions to slightly larger rates than those reported by Stancil *et al.* [13] and Schleicher *et al.* [12].

In their QCT calculation, Esposito *et al.* [2] perform the final analysis by the HB technique, indicating that the title reaction, as opposed to the reverse process He + H_2^+, is not affected by ZPE issues or the specific choice of the binning procedure. Our results, on the contrary, suggest that the application of the GB yield differences with respect to the HB, especially the rate constants as shown in Figures 6 and 7. Discrepancies between both approaches seem to increase with the vibrational excitation of the product $H_2^+(v')$ and, in most of the cases, a better agreement with the QM results is seen for the GB case.

V. CONCLUSIONS

The dynamics of the H + $HeH^+ \rightarrow$ He + H_2^+ reaction has been investigated by means of a SQM, RPMD and QCT calculations. Up to our knowledge this is the first time the title process is studied to see the role played by complex-forming mechanisms, a pathway previously observed in reactions with similar potential wells in the intermediate region. The statistical predictions certainly reproduce some of the overall features observed in both cross sections and rate constants observed in previous QM studies but a state-to-state analysis reveals certain inversion in the population of the vibrationally excited $H_2^+(v' > 0)$ states. Moreover, the QCT analysis reveals that the calculated complex lifetimes are too short to expect a purely statistical dynamics. We have found the convenience of the GB procedure in the analysis performed within the QCT calculation. The RPMD approach has shown to yield rate constants in good agreement over the entire temperature range under consideration, down as low as 10 K, as long as the R_∞ parameter is set far enough (about 3-4 times the

maximum impact parameter foudn in the QCT calculation.

VI. ACKNOWLEDGMENTS

T.G.L. would like to thank support from the MINECO with Grant No FIS2017-83157-P. This work was supported by the "Programme National Physique et Chimie du Milieu Interstellaire" (PCMI) of CNRS/INSU with INC/INP co-funded by CEA and CNES. Y.S. would like to thank support from the High Performance Computing Platform MESO@LR at the University of Montpellier, and from the Computing Center of the "Institut National de Physique Nucléaire" (IN2P3) is acknowledged. Y.V.S. and S.B. acknowledge the support of the European Regional Development Fund and the Republic of Cyprus through the Research Promotion Foundation (Projects: INFRASTRUCTURE/1216/0070 and Cy-Tera ΝΕΑ ΥΠΟΔΟΜΗ/ΣΤΡΑΤΗ/0308/31).

TABLE I: Input parameters for the RPMD calculations on the H + HeH^+ reaction

		Description
Potential energy surface		Ref. [23]
Command line parameters		
`Temp`	10, 20, 30, 50, 75, 100, 150,	Temperature (K)
	200, 300, 400, 500, 600	
`Nbeads`	512 (10 K−100 K)	Number of beads
	256 (150 K−200 K)	
	128 (300 K−600 K)	
Dividing surface parameters		
R_∞	50 (10 K−20 K)	Asymptotic distance between
	40 (30 K−75 K)	the reactants (a_0)
	30 (100 K−600 K)	
N_{bonds}	1	Number of forming and breaking bonds
N_{channel}	1	Number of equivalent product channels
He	[0.00, 0.00, -1.93]	Cartesian coordinate of the
H	[0.00, 0.00, 0.00]	intermediate geometry (a_0)
H	[0.00, 0.00, 2.07]	
`Thermostat`	'Andersen'	Thermostat option
Biased sampling parameters		
N_{windows}	111	Number of windows
ξ_1	−0.05	Center of the first window
$d\xi$	0.01	Window spacing step
ξ_N	1.05	Center of the last window
dt	0.0001	Time step (ps)
k_i	2.72 − 21.77	Umbrella force constant ((T/K) eV)
$N_{\mathrm{trajectory}}$	100	Number of trajectories
$t_{\mathrm{equilibration}}$	20	Equilibration period (ps)
t_{sampling}	100	Sampling period in each trajectory (ps)
Potential of mean force calculation		
ξ_0	−0.050	Start of umbrella integration
$\xi^\ddagger$	0.74 (100 K)[b], 0.75 (10, 150 K)[b]	End of umbrella integration
	0.76 (30, 200, 300 K)[b], 0.78 (20, 400, 500 K)[b]	
	0.79 (600 K)[b], 0.80 (50, 75 K)[b]	
N_{bins}	4999	Number of bins
Recrossing factor calculation		
dt	0.0001	Time step (ps)
$t_{\mathrm{equilibration}}$	20	Equilibration period (ps) of parent trajectories
$\mathrm{N}_{\mathrm{totalchild}}$	100 000	Number of unconstrained (child) trajectories
$t_{\mathrm{childsampling}}$	2	Sampling increment along the parent trajectories (ps)
$\mathrm{N}_{\mathrm{child}}$	100	Number of child trajectories per
		one initially constrained configuration
t_{child}	1.5	Length of child trajectories (ps)

[a] The explanation of the format of the input file can be found in the RPMDrate code manual (`http://rpmdrate.cyi.ac.cy`).

[b] Detected automatically by RPMDrate.

TABLE II: Total and vibrationally-resolved cross sections for the H+HeH$^+$($v = 0, j = 0$) $\rightarrow$ $H_2^+(v')$+He for different values of the collision energy by means of the present SQM and QCT calculations and the QM[2]. Units are in Å^2.

$E_c = 0.001$ eV	$\sigma_{\rm tot}$	$\sigma_{v'=0}$	$\sigma_{v'=1}$	$\sigma_{v'=2}$	$\sigma_{v'=3}$
QM	5.44	0.90	1.87	1.89	0.79
QCT	0.08	0.01	0.02	0.04	0.01
SQM	2.45	0.98	0.79	0.53	0.14
$E_c = 0.01$ eV	$\sigma_{\rm tot}$	$\sigma_{v'=0}$	$\sigma_{v'=1}$	$\sigma_{v'=2}$	$\sigma_{v'=3}$
QM	45.74	5.97	12.23	17.76	9.78
QCT	18.08	2.98	5.82	6.69	2.59
SQM	48.44	19.91	15.50	10.50	2.52
$E_c = 0.1$ eV	$\sigma_{\rm tot}$	$\sigma_{v'=0}$	$\sigma_{v'=1}$	$\sigma_{v'=2}$	$\sigma_{v'=3}$
QM	30.95	4.79	10.37	9.46	6.35
QCT	28.84	4.76	8.53	9.95	5.61
SQM	33.65	15.53	10.55	5.88	1.68

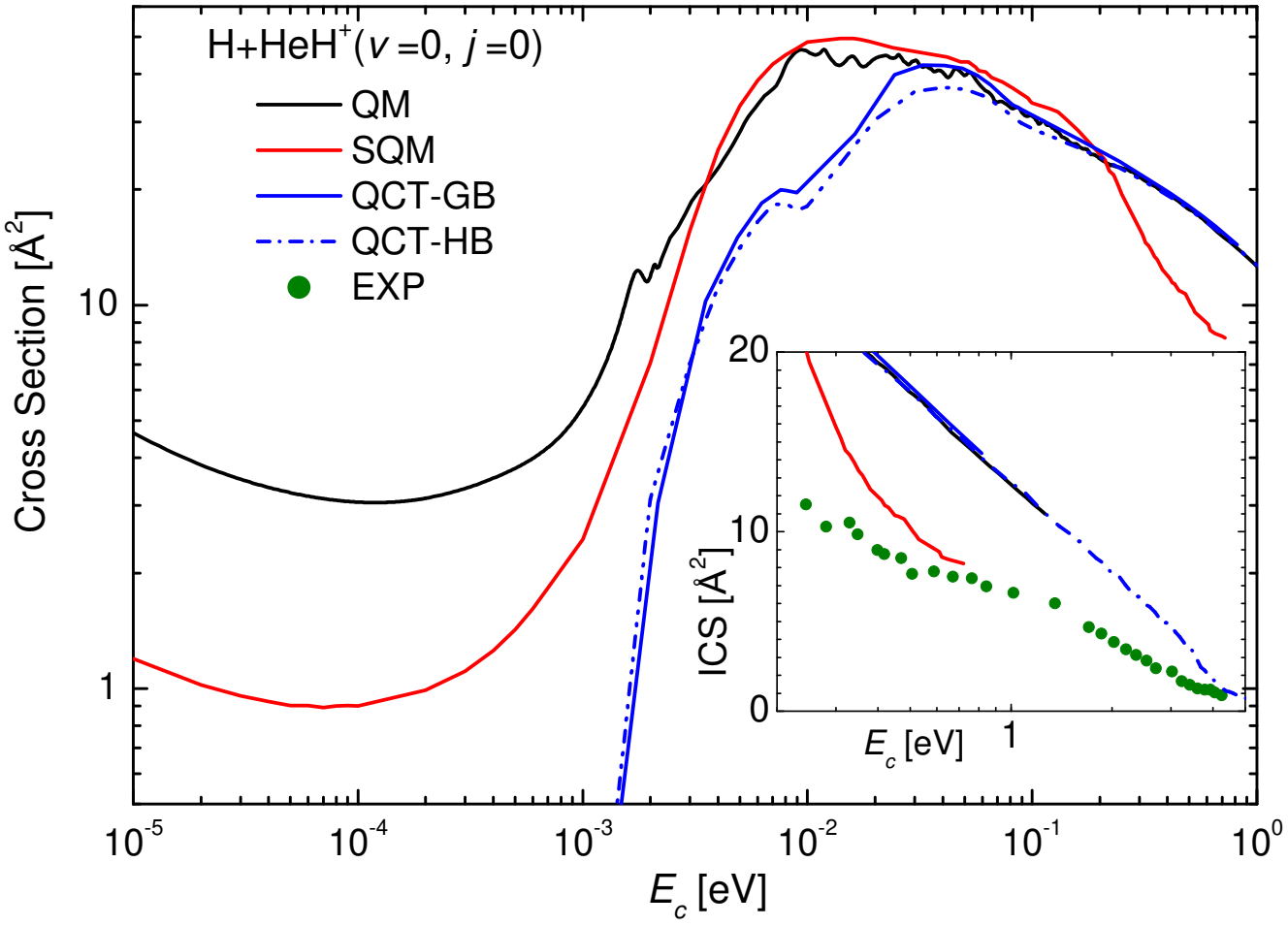

FIG. 1: Integral cross sections for the H+HeH$^+$($v = 0, j = 0$) $\rightarrow$ He+H$_2^+$ reaction as a function of the collision energy calculated here with the SQM (red) and QCT-GB (solid blue) methods and compared with the QM (black) and QCT-HB (blue dashed-dotted) calculations of Ref. [2]. Units are Å^2. In the inset we show the similar comparison for the collision energy range $E_c \geq 0.2$ eV including the experimental values from Ref. [50] (green circles)

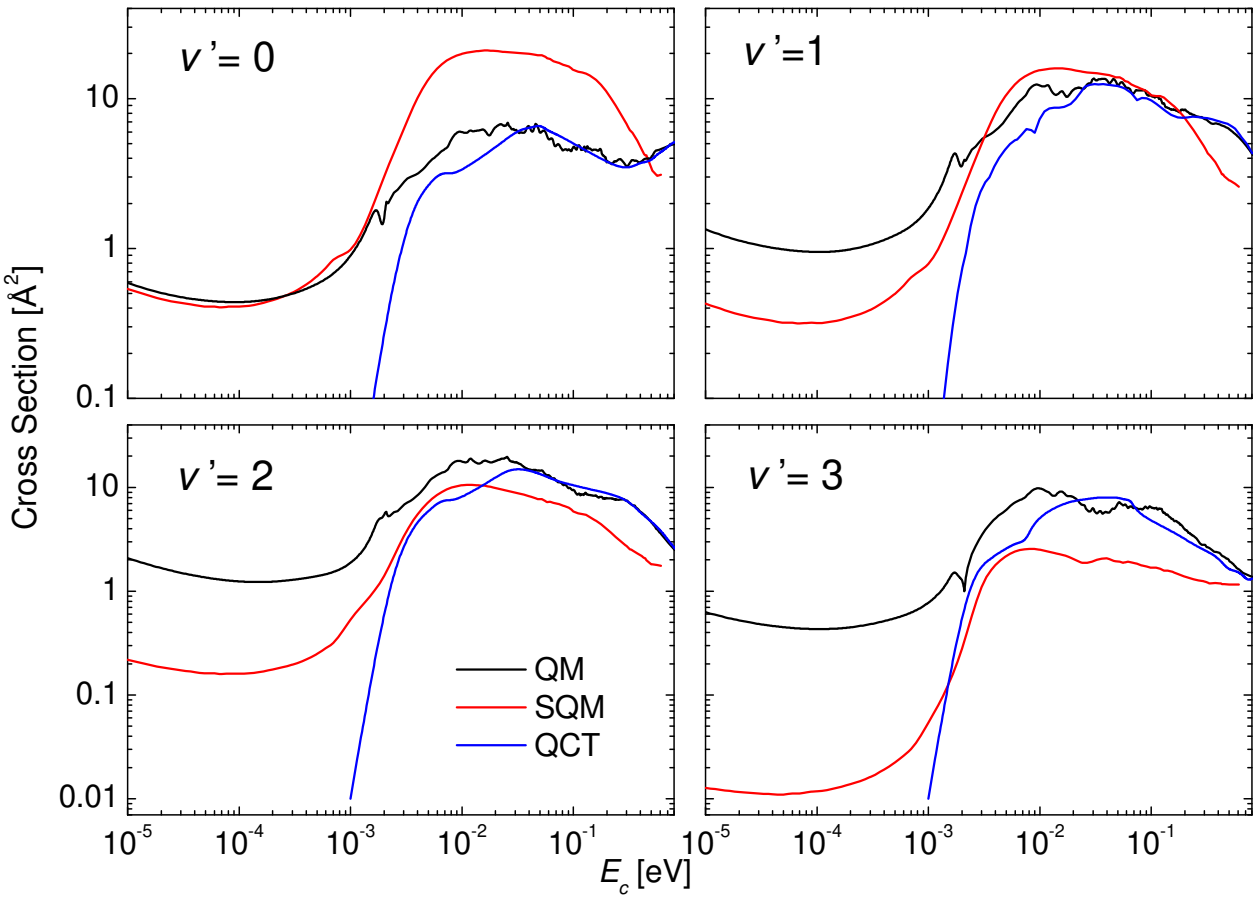

FIG. 2: State-to-state integral cross sections in Å^2 for the H+HeH$^+$($v = 0, j = 0$) $\rightarrow$ He+H$_2^+$($v' = 0 - 3$) processes for collision energy between 10^{-5} and 0.7 eV in logarithmic scales. QM (black) results from Ref. [2] are compared with present SQM (red) and QCT (blue) cross sections.

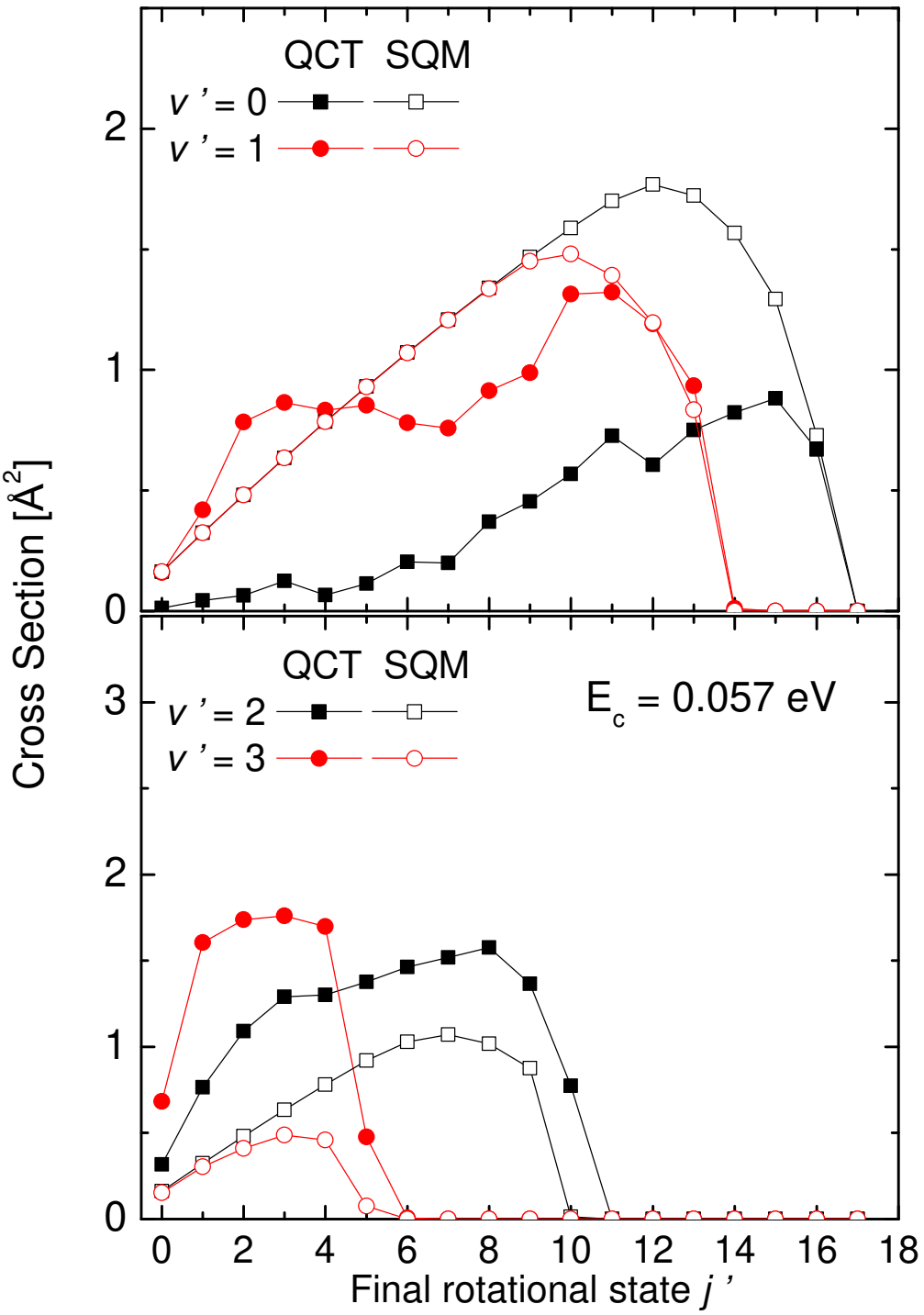

FIG. 3: Rotational distributions for the state-to-state H+HeH$^+$($v = 0, j = 0$) $\rightarrow$ He+H$_2^+$(v', j') reactions at $E_c = 0.057$ eV. QCT (full symbols) and SQM (open symbols) cross sections in Å^2 are compared for $v' = 0, 1$ (top panel) and $v' = 2, 3$ (bottom panel).

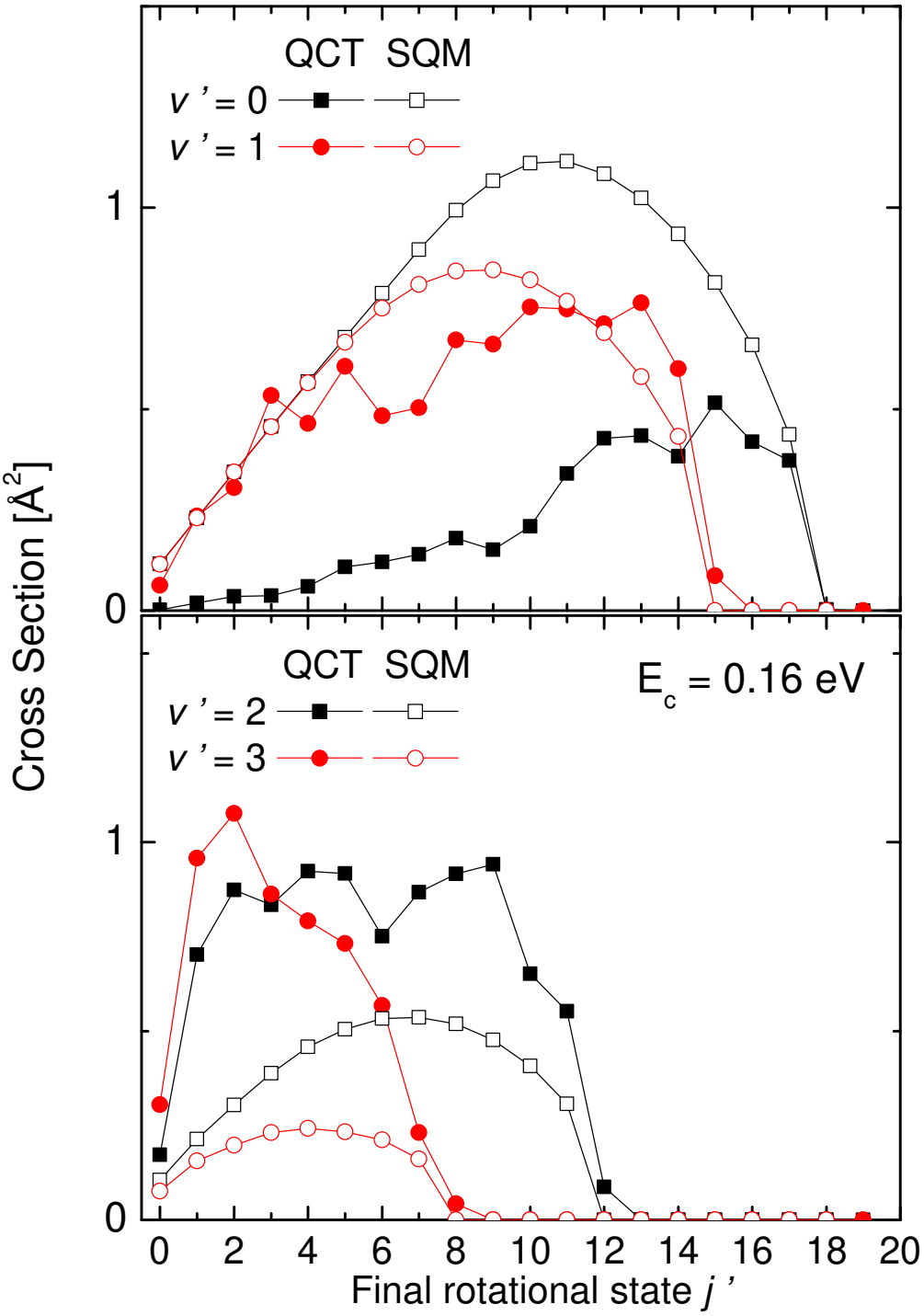

FIG. 4: Same as Fig. 3 for $E_c = 0.16$ eV.

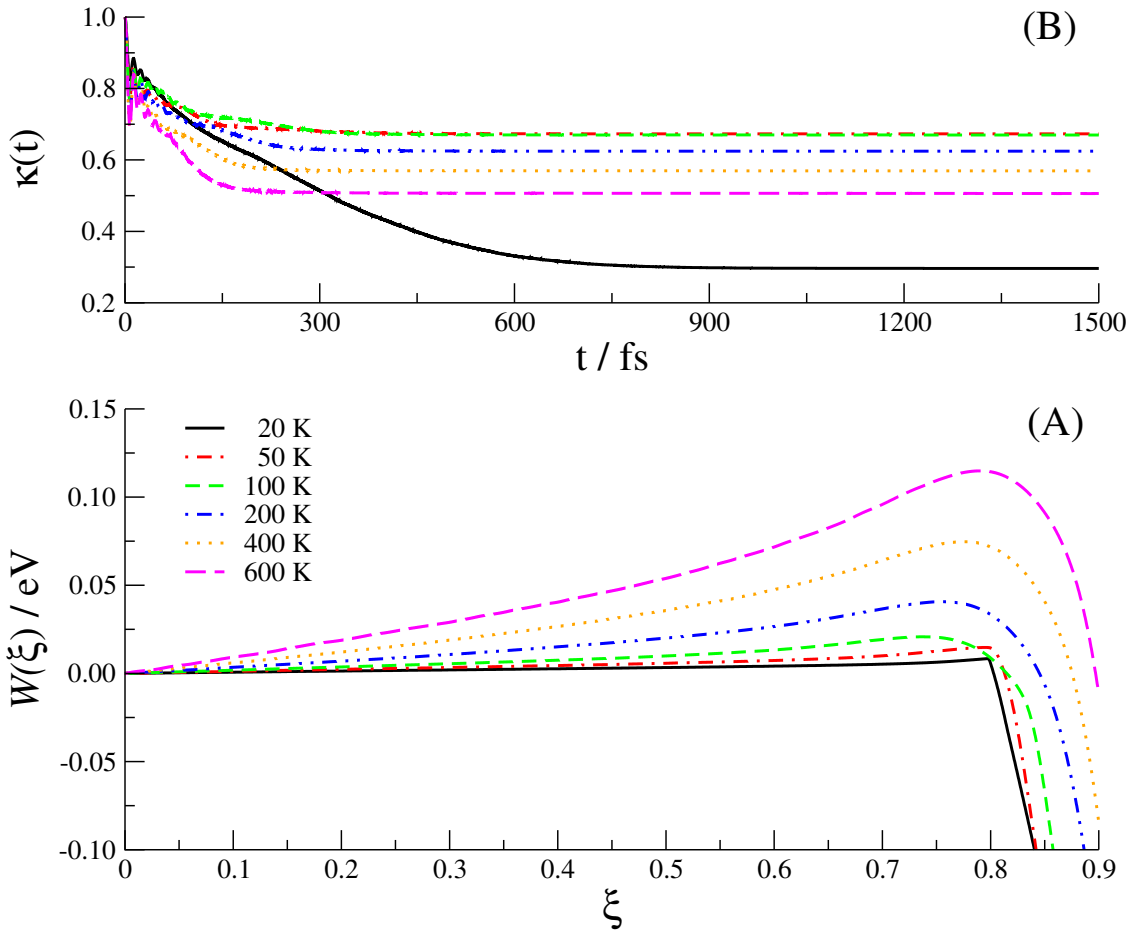

FIG. 5: (A) Variation of the RPMD potential of mean force, $W(\xi)$, (in eV) along the reaction coordinate ξ for the temperature range 10 K−600 K. (B) RPMD time dependent transmission coefficient, $\kappa(t)$, in the temperature range 10 K−600 K. The legends correspond to both (A) and (B).

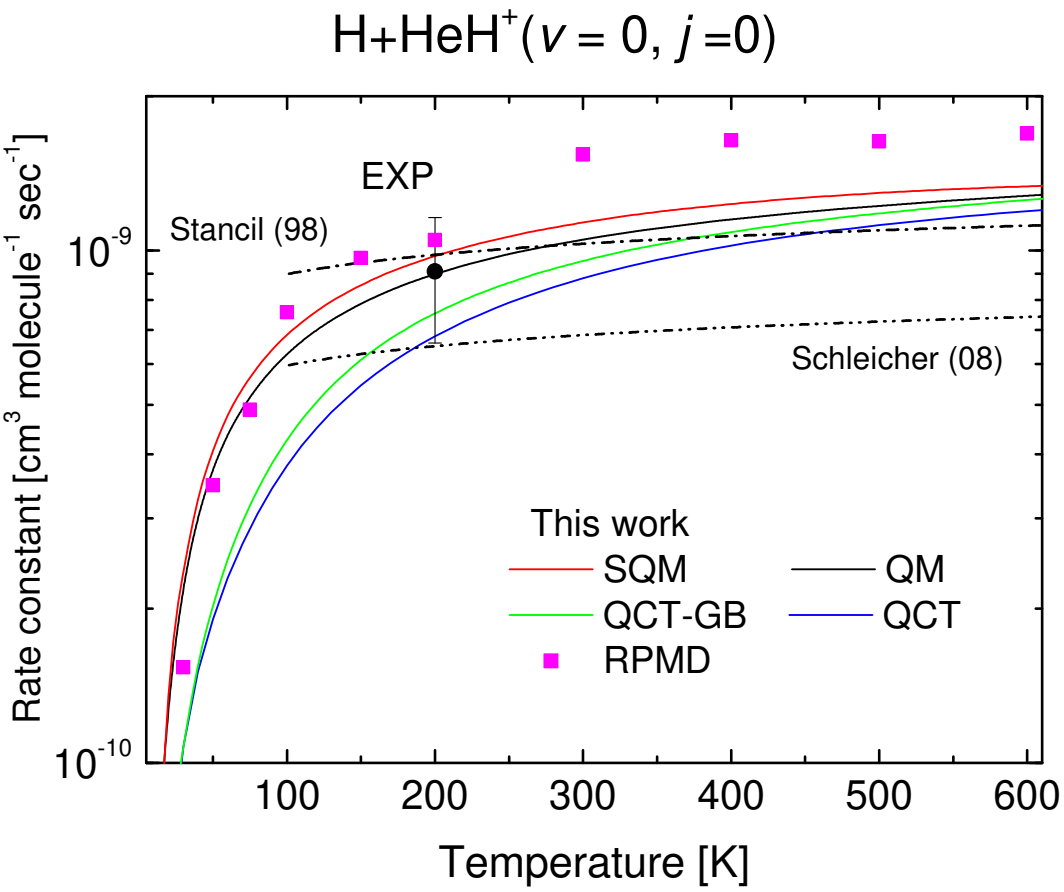

FIG. 6: Rate constants for the H+HeH$^+$($v = 0, j = 0$) $\rightarrow$ He+H$_2^+$ reaction obtained in this work with the RPMD (magenta squares), SQM (red line) and QCT with the Gaussian-binning procedure (green line). Present results are compared with QM (black line) and QCT with histogram-binning (blue lines) from Ref. [2]. The experimental result at $T = 200$ K by Karpas *et al.* [15] (black circle with error bars) and rate constants from Refs. [13] (dashed-dotted line) and [12] (dashed-dotted-dotted line) are also included for comparison.

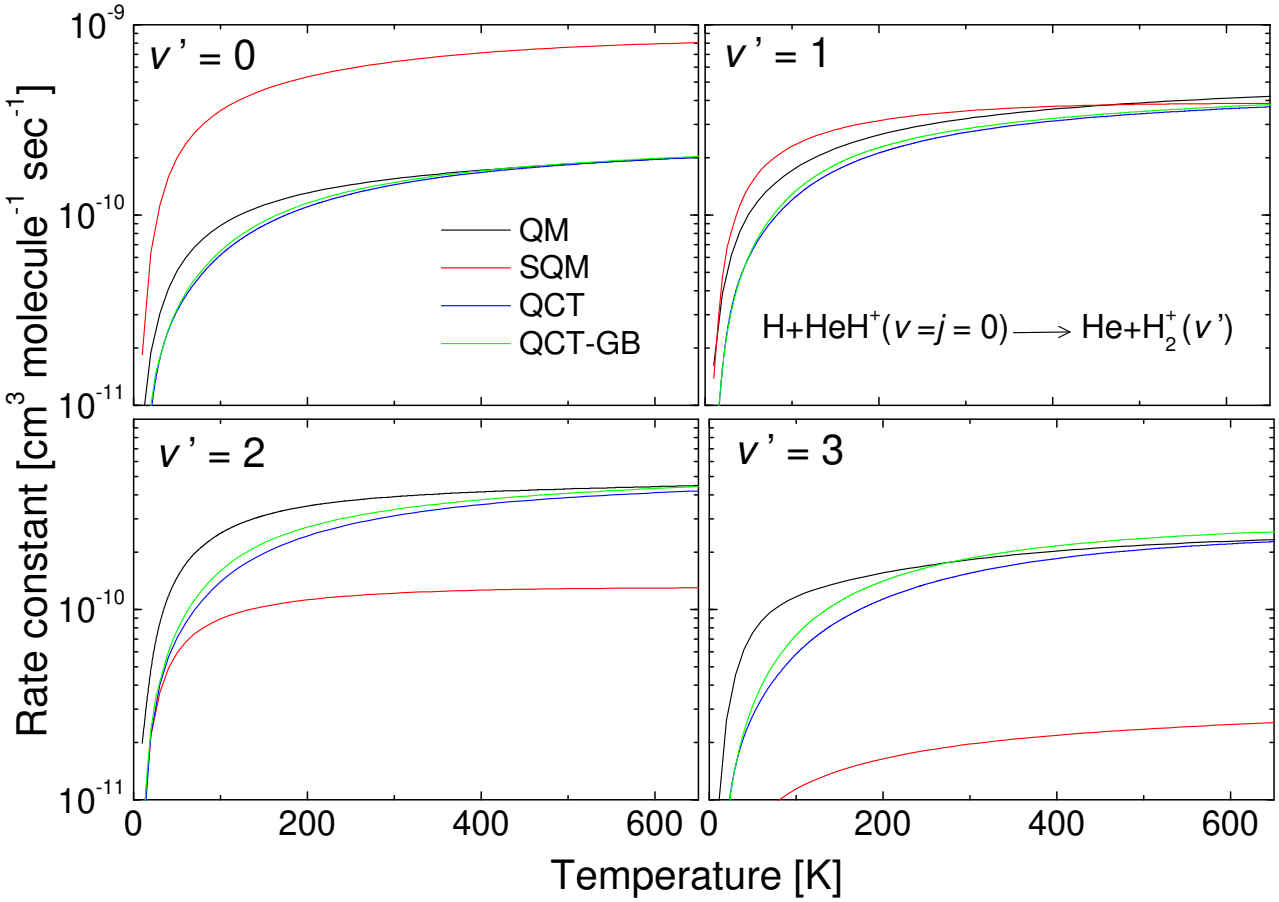

FIG. 7: Comparison of state-to-state rate constants for the H+HeH$^+$($v = 0, j = 0$) $\rightarrow$ He+H$_2^+$(v') reaction obtained with present SQM (red line) and QCT with the Gaussian-binning methods (green line) and those from Ref. [2] calculated with a QM (black line) and QCT (blue lines) calculations.

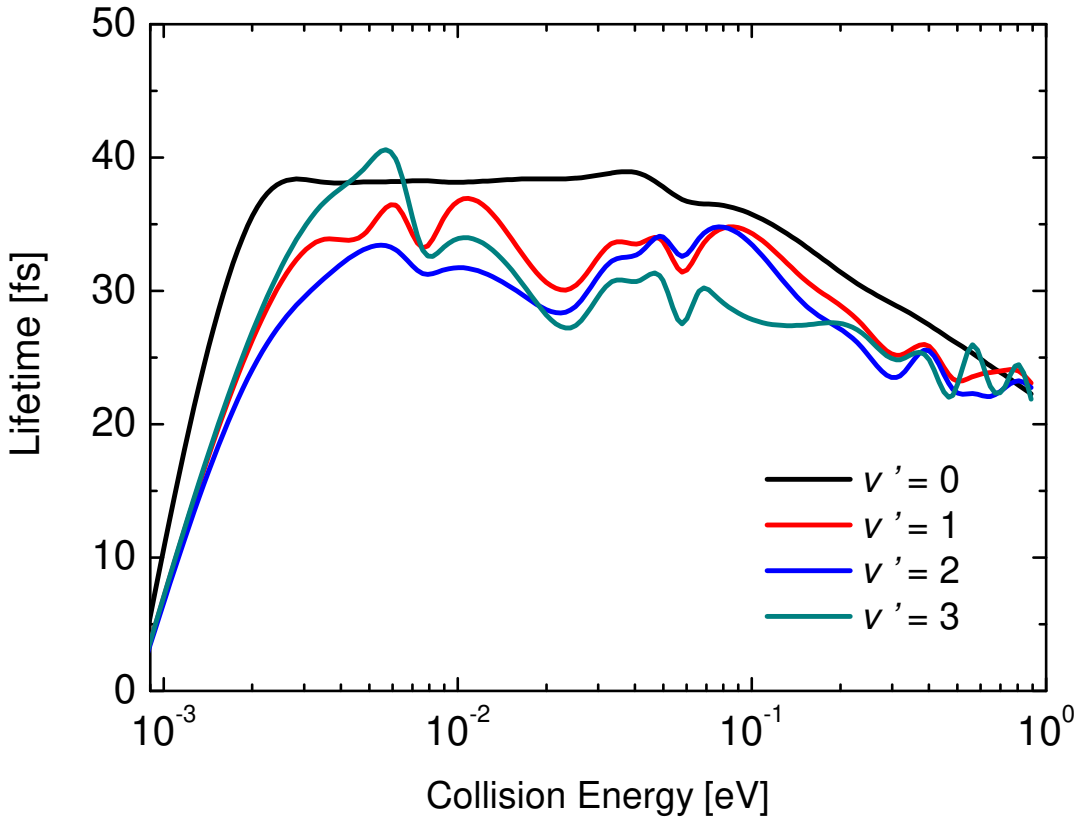

FIG. 8: Collision average lifetimes in fs obtained with present QCT calculation for the $H+HeH^+(v=0,j=0) \rightarrow He+H_2^+(v'=0-3)$ reaction.

[1] Güsten, R.; Wiesemeyer, H.; Neufeld, D.; Menten, K. M.; Graf, U. U.; Jacobs, K.; Klein, B.; Ricken, Risacher, C.; Stutzki, J. Astrophysical Detection of the Helium Hydrude Ion HeH^+ *Nature* **2019**, *568*, 357–359.

[2] Esposito, F.; Coppola, C. M.; De Fazio, D. Complementarity between Quantum and Classical Mechanics in Chemical Modeling. The H + $HeH^+ \rightarrow H_2^+$ + He Reaction: A Rigourous Test for Reaction Dynamics Methods *J. Phys. Chem. A* **2015**, *119*(51), 12615–12626.

[3] Gamallo, P.; Akpinar, S.; Defazio, P.; Petrongolo, C. Quantum Dynamics of the Reaction $H(^2S)$ + $HeH^+(X^1\Sigma^+) \rightarrow H_2$+$(X^2\Sigma_g^+)$ + $He(^1S)$ from Cold to Hyperthermal Energies: Time-Dependent Wavepacket Study and Comparison with Time-Independent Calculations *J. Phys. Chem. A* **2014**, *118*(33), 6451–6456.

[4] De Fazio, D. The H + $HeH^+ \rightarrow$ He + H_2^+ Reaction from the Ultra-cold Regime to the Three-body Breakup: Exact Quantum Mechanical Integral Cross Sections and Rate Constants *Phys. Chem. Chem. Phys.* **2014**, *16*, 11662–11672.

[5] Bovino, S.; Gianturco, F.; Tacconi, M. Chemical Destruction of Rotationally 'Hot' HeH^+: Quantum Cross Sections and Mechanisms of its Reaction with H *Chem. Phys. Lett.* **2012**, *554*, 47 – 52.

[6] Bovino, S.; Tacconi, M.; Gianturco, F. A. Cold Chemistry with Ionic Partners: Quantum Features of $HeH^+(^1\Sigma)$ with $H(^1S)$ at Ultralow Energies *J. Phys. Chem. A* **2011**, *115*(29), 8197–8203.

[7] De Fazio, D.; de Castro-Vitores, M.; Aguado, A.; Aquilanti, V.; Cavalli, S. The He + $H_2^+ \rightarrow$ HeH^+ + H Reaction: Ab Initio Studies of the Potential Energy Surface, Benchmark Time-Independent Quantum Dynamics in an Extended Energy Range and Comparison with Experiments *J. Chem. Phys.* **2012**, *137*(24), 244306.

[8] Tang, X. N.; Xu, H.; Zhang, T.; Hou, Y.; Chang, C.; Ng, C. Y.; Chiu, Y.; Dressler, R. A.; Levandier, D. J. A Pulsed-field Ionization Photoelectron Secondary Ion Coincidence Study of the $H_2^+(X, \nu^+ = 015, N^+ = 1)$+He Proton Transfer Reaction *J. Chem. Phys.* **2005**, *122*(16), 164301.

[9] Panda, A. N.; Sathyamurthy, N. Time-dependent Quantum Mechanical Wave Packet Study of the He+$H_2^+(v, j) \rightarrow$ HeH^++H Reaction *J. Chem. Phys.* **2005**, *122*(5), 054304.

[10] Liang, J.; Liu, X.; Xu, W.; Kong, H.; Zhang, Q. Isotopic Effect on Stereodynamics of the Reactions of H+HeH^+/H+HeD^+/H+HeT^+ *J. Mol. Struct. THEOCHEM* **2010**, *942*(1), 93 – 97.

[11] Bovino, S.; Tacconi, M.; Gianturco, F. A.; Galli, D. Ion Chemistry in the Early Universe - Revisiting the Role of HeH^+ with New Quantum Calculations *A&A* **2011**, *529*, A140.

[12] Schleicher, D. R. G.; Galli, D.; Palla, F.; Camenzind, M.; Klessen, R. S.; Bartelmann, M.; Glover, S. C. O. Effects of Primordial Chemistry on the Cosmic Microwave Background *A&A* **2008**, *490*(2), 521–535.

[13] Stancil, P. C.; Lepp, S.; Dalgarno, A. The Deuterium Chemistry of the Early Universe *Astrophys. J.* **1998**, *509*(1), 1–10.

[14] Galli, D.; Palla, F. The Chemistry of the Early Universe *A&A* **1998**, *335*, 403.

[15] Karpas, Z.; Anicich, V.; Huntress, W. T. An Ion Cyclotron Resonance Study of Reactions of Ions with Hydrogen Atoms *J. Chem. Phys.* **1979**, *70*(6), 2877–2881.

[16] Linder, F.; Janev, R. K.; Botero, J. Linder, F.; Janev, R. K.; Botero, J. Reactive Ion-molecule Collisions Involving Hydrogen and Helium In *Atomic and Molecular Processes in Fusion Edge Plasmas*; Janev, R. K., Ed.; Springer US: Boston, MA, 1995; pages 397–431.

[17] McLaughlin, D. R.; Thompson, D. L. Ground and Lower Excited State Discrete Ab Initio Electronic Potential Energy Surfaces for Doublet HeH_2^+ *J. Chem. Phys.* **1979**, *70*(6), 2748–2769.

[18] Joseph, T.; Sathyamurthy, N. Dynamics of the Endothermic Reaction He+$H_2^+ \rightarrow HeH^+ + H$ on an Accurate Ab Initio Potentialenergy Surface *J. Chem. Phys.* **1987**, *86*(2), 704–714.

[19] Aguado, A.; Paniagua, M. A New Functional Form to Obtain Analytical Potentials of Triatomic Molecules *J. Chem. Phys.* **1992**, *96*(2), 1265–1275.

[20] Aguado, A.; Suárez, C.; Paniagua, M. Accurate Fit of the Two Lowest Excited State Potential Energy Surfaces for Doublet HeH_2^+ *J. Chem. Phys.* **1993**, *98*(1), 308–315.

[21] Palmieri, P.; Puzzarini, C.; Aquilanti, V.; Capecchi, G.; Cavalli, S.; Fazio, D. D.; Aguilar, A.; Giménez, X.; Lucas, J. M. Ab Initio Dynamics of the He + $H_2^+ \rightarrow HeH^+ + H$ Reaction: a New Potential Energy Surface and Quantum Mechanical Cross-sections *Mol. Phys.* **2000**, *98*(21), 1835–1849.

[22] Aquilanti, V.; Capecchi, G.; Cavalli, S.; Fazio, D. D.; Palmieri, P.; Puzzarini, C.; Aguilar, A.; Giménez, X.; Lucas, J. The He + H_2^+ Reaction: a Dynamical Test on Potential Energy

Surfaces for a System Exhibiting a Pronounced Resonance Pattern *Chem. Phys. Lett.* **2000**, *318*(6), 619 – 628.

[23] Ramachandran, C.; Fazio, D. D.; Cavalli, S.; Tarantelli, F.; Aquilanti, V. Revisiting the Potential Energy Surface for the He+H_2^+ $\rightarrow$ HeH^+ + H Reaction at the Full Configuration Interaction Level *Chem. Phys. Lett.* **2009**, *469*(1), 26 – 30.

[24] Koner, D.; Barrios, L.; González-Lezana, T.; Panda, A. N. Wave Packet and Statistical Quantum Calculations for the He + NeH^+ $\rightarrow$ HeH^+ + Ne Reaction on the Ground Electronic State *J. Chem. Phys.* **2014**, *141*(11), 114302.

[25] Koner, D.; Barrios, L.; González-Lezana, T.; Panda, A. N. Scattering Study of the Ne + $NeH^+(v_0 = 0, j_0 = 0)$ $\rightarrow$ NeH^+ + Ne Reaction on an Ab Initio Based Analytical Potential Energy Surface *J. Chem. Phys.* **2016**, *144*(3), 034303.

[26] Koner, D.; Barrios, L.; González-Lezana, T.; Panda, A. N. State-to-State Dynamics of the Ne + $HeH^+(v = 0, j = 0)$ $\rightarrow$ $NeH^+(v', j')$ + He Reaction *J. Phys. Chem. A* **2016**, *120*(27), 4731–4741.

[27] Koner, D.; Barrios, L.; González-Lezana, T.; Panda, A. N. Quantum, Statistical, and Quasiclassical Trajectory Studies For the Ne + HeH^+ $\rightarrow$ NeH^+ + He Reaction on the Ground Electronic State *J. Phys. Chem. A* **2015**, *119*(50), 12052–12061.

[28] Rackham, E. J.; Huarte-Larrañaga, F.; Manolopoulos, D. E. Coupled-channel Statistical Theory of the N(^2D)+H_2 and O(^1D)+H_2 Insertion Reactions *Chem. Phys. Lett.* **2001**, *343*(34), 356–364.

[29] Rackham, E. J.; González-Lezana, T.; Manolopoulos, D. E. A Rigorous Test of the Statistical Model for Atom–diatom Insertion Reactions *J. Chem. Phys.* **2003**, *119*, 12895.

[30] González-Lezana, T. Statistical Quantum Studies on Insertion Atom-diatom Reactions *Int. Rev. Phys. Chem.* **2007**, *26*, 29.

[31] Bonnet, L.; Larrégaray, P.; Rayez, J. C.; González-Lezana, T. Parity Conservation and Polarization of Differential Cross Sections in Complex-forming Chemical Reactions *Phys. Chem. Chem. Phys.* **2006**, *8*, 3951.

[32] Bargueño, P.; González-Lezana, T.; Larrégaray, P.; Bonnet, L.; Claude Rayez, J. Time Dependent Wave Packet and Statistical Calculations on the H + O_2 Reaction *Phys. Chem. Chem. Phys.* **2007**, *9*(9), 1127–1137.

[33] Dayou, F.; Larrégaray, P.; Bonnet, L.; Rayez, J.-C.; Arenas, P. N.; González-Lezana, T.

A Comparative Study of the Si + O_2 → SiO + O Reaction Dynamics from Quasiclassical Trajectory and Statistical Based Methods *J. Chem. Phys.* **2008**, *128*, 174307.

[34] Bossion, D.; Scribano, Y.; Lique, F.; Parlant, G. Ro-vibrational Excitation of H_2 by H Extended to High Temperatures *Mon. Not. R. Astron. Soc.* **2018**, *480*, 3718–3724.

[35] Bossion, D.; Scribano, Y.; Parlant, G. State-to-state Quasi-classical Trajectory Study of the D + H_2 Collision for High Temperature Astrophysical Applications *J. Chem. Phys.* **2019**, *150*, 084301.

[36] Berry, M. V.; Mount, K. E. Semiclassical Approximations in Wave Mechanics *Rep. Prog. Phys.* **1972**, *35*, 315.

[37] Truhlar, D. G.; Muckerman, J. T. *Atom-molecule Collision Theory: A Guide for the Experimentalist;* R. B. Bernstein, 1979.

[38] Karplus, M.; Porter, R. N.; Sharma, R. D. Exchange Reactions with Activation Energy. I. Simple Barrier Potential for (H,H_2) *J. Chem. Phys.* **1965**, *43*, 3259.

[39] Bonnet, L.; Rayez, J.-C. Quasiclassical Trajectory Method for Molecular Scattering Processes: Necessity of a Weighted Binning Approach *Chem. Phys. Lett.* **1997**, *277*, 183–190.

[40] Bonnet, L.; Espinosa-García, J. The Method of Gaussian Weighted Trajectories. V. On the 1GB Procedure for Polyatomic Processes *J. Chem. Phys.* **2010**, *133*, 164108.

[41] Habershon, S.; Manolopoulos, D.E, Markland, T. E., Miller III, T.F. Ring-Polymer Molecular Dynamics: Quantum Effects in Chemical Dynamics from Classical Trajectories in an Extended Phase Space *Ann. Rev. Phys. Chem.* **2013**, *64*, 387–413.

[42] Bhowmick, S.; Bossion, D.; Scribano, Y.; Suleimanov, Y. The low temperature D^+ + H_2 → HD + H^+ Reaction Rate Coefficient: A Ring Polymer Molecular Dynamics and Quasi-classical Trajectory Study *Phys. Chem. Chem. Phys.*. **2018**, *20*, 26752.

[43] Collepardo-Guevara, R.; Suleimanov, Y.; Manolopoulos, D. Bimolecular Reaction Rates from Ring Polymer Molecular Dynamics *J. Chem. Phys.* **2009**, *130*, 174713.

[44] Suleimanov, Y.; Collepardo-Guevara, R.; Manolopoulos, D. Bimolecular Reaction Rates from Ring Polymer Molecular Dynamics: Application to H + CH_4 → H_2 + CH_3 *J. Chem. Phys.* **2011**, *134*, 044131.

[45] Suleimanov, Y.; Aoiz, F.; Guo, H. Chemical Reaction Rate Coefficients from Ring Polymer Molecular Dynamics: Theory and Practical Applications *J. Phys. Chem. A* **2016**, *120*, 8488–8502.

[46] Suleimanov, Y.; Allen, J.; Green, W. RPMDrate: Bimolecular Chemical Reaction Rates from Ring Polymer Molecular Dynamics *Comput. Phys. Comm.* **2013**, *184*, 833–840.

[47] Kästner, J.; Thiel, W. Bridging the Gap Between Thermodynamic Integration and Umbrella Sampling Provides a Novel Analysis Method: Umbrella Integration *J. Chem. Phys.* **2005**, *123*(14), 144104.

[48] Kästner, J.; Thiel, W. Analysis of the Statistical Error in Umbrella Sampling Simulations by Umbrella Integration *J. Chem. Phys.* **2006**, *124*(23), 234106.

[49] Andersen, H. Molecular Dynamics Simulations at Constant Pressure and/or Temperature *J. Chem. Phys.* **1980**, *72*, 2384.

[50] Rutherford, J. A.; Vroom, D. A. Study of the Reactions $H_2^+ + He \rightarrow HeH^+ + H$ and $HeH^+ + H \rightarrow H_2^+ + He$ Using Crossed Beam Techniques *J. Chem. Phys.* **1973**, *58*(10), 4076–4079.

[51] Rampino, S.; Suleimanov, Y. V. Thermal Rate Coefficients for the Astrochemical Process $C + CH^+ \rightarrow {C_2}^+ + H$ by Ring Polymer Molecular Dynamics *J. Phys. Chem. A* **2016**, *120*, 9887–9893.

[52] Hickson, K. M.; Loison, J.-C.; Guo, H.; Suleimanov, Y. V. Ring-polymer Molecular Dynamics for the Prediction of Low-Temperature Rates: an Investigation of the $C(^1D) + H_2$ Reaction *J. Phys. Chem. Lett.* **2015**, *6*, 4194–4199.

[53] Hickson, K. M.; Suleimanov, Y. V. Low-temperature Experimental and Theoretical Rate Constants for the $O(^1D) + H_2$ Reaction *J. Phys. Chem. A* **2017**, *121*, 1916–1923.